Journal of Hydroscience and Hydraulic Engineering
Vol. 25, No.1 May, 2007, 31-39

THREE DIMENSIONAL COMPUTATIONAL METHOD FOR WAVE FLOWS RUNNING UP IN A RIVER AND THEIR FLOODED FLOWS

By

Satoru Ushijima

Department of Civil and Earth Resources Engineering, Kyoto University, Kyoto-shi, 615-8540, Japan

Osashi Makino

Department of Civil and Earth Resources Engineering, Kyoto University, Kyoto-shi, 615-8540, Japan

and

Iehisa Nezu

Department of Civil and Earth Resources Engineering, Kyoto University, Kyoto-shi, 615-8540, Japan

SYNOPSIS

It has been actually observed that the wave flows due to tsunamis, which have reached river mouths, sometimes become running-up flows in rivers. As a result, they cause serious damage to structures. A three-dimensional computational method based on MICS (Multiphase Incompressible flow solver with Collocated grid System) is being planned to be used to evaluate the related local phenomena caused by the running-up flows, such as the transportation of floating materials, fluid forces acting on structures and flooded flows over river banks, since MICS enables us to deal with the front of free surface flows accurately and evaluate fluid forces against solid objects without empirical formulations. In this paper, some hydraulic experiments were conducted with a flume equipped with a wave generator and some fixed boxes which simulate a waterway, coastal levees and the land areas. The computational method based on MICS was applied to the experimental results and its validity was discussed by comparing the experimental and computational results.

INTRODUCTION

It has been reported that the wave flows caused by tsunamis, which can reach river mouths, often run up along rivers in the upstream direction and are sometimes transformed into flows accompanied by drifting things which cause serious damage to structures in the rivers, like bridge piers. In addition, when the running-up flows overflow the river embankments, the flows can extend to residential, industrial and other important areas causing disasters such as floods.

It is therefore important to understand the characteristics of the running-up wave flows, transportation of drifting objects and the behaviors of their flooded flows, in order to predict the possible damage in the related areas and to plan for evacuation procedures. According to previous studies of flooded flows due to tsunamis(1), it was pointed out that the sufficient spatial resolution is necessary in the numerical predictions with shallow water equations. In addition, a numerical study was conducted using one-dimensional shallow water equation with nonlinear dispersive wave theory for the propagation of tsunami in rivers (2). In fact, a high-resolution and three-dimensional computational method is essentially important to evaluate the transportation of drifting objects and the forces acting on the structures due to wave flows and collisions of the objects, since these local

phenomena have three-dimensional characteristics that cannot be treated with two-dimensional shallow water equations.

Taking account of the above indications, the 3D MICS(3) (Multiphase Incompressible flow solver with Collocated grid System) is thought to be one of the most effective computational methods, since it enables us to predict multiphase flow fields, such as the transportation of solid objects in free-surface flows. It has been confirmed that the 3D MICS enables us to predict the movements of objects due to wave flows and to evaluate the fluid forces acting on the objects without any empirical formulations, such as the coefficient of resistant force(3).

In this paper, some basic hydraulic experiments were conducted using a flume by means of a wave generator to measure the running-up flows in a waterway and their flooded flows over land areas. In addition, the computational method based on the 3D MICS was applied to the experimental results to confirm its validity. Conclusively, the applicability of the 3D MICS is discussed by making a comparison between the experimental and the computational results.

NUMERICAL PROCEDURES

Basic equations

The governing equations used in MICS are based on a one-fluid model which is similar to that of mixture gas. In the MICS, the multiphase field is assumed to be constructed with immiscible and incompressible fluids with different physical properties. The details of the derivation and modelings concerning the governing equations can be found in our previous paper(3). The governing equations consist of the following mass preservation law written in the Euler description, incompressible condition and momentum equations:

$$\frac{\partial \rho}{\partial t} + \frac{\partial}{\partial x_j}(\rho u_j) = 0 \tag{1}$$

$$\frac{\partial u_j}{\partial x_j} = 0 \tag{2}$$

$$\frac{\partial u_i}{\partial t} + \frac{\partial}{\partial x_j}(u_i u_j) = f_i + f_{s,i} - \frac{1}{\rho}\frac{\partial p}{\partial x_i} + \frac{1}{\rho}\frac{\partial}{\partial x_j}\left[\frac{\partial}{\partial x_j}(\mu u_i) + \frac{\partial}{\partial x_i}(\mu u_j)\right] \tag{3}$$

where ρ is the volume-averaged density in the control volume that is a sufficiently small volume including different incompressible fluids. While the pressure p and coefficient of viscosity μ are volume-averaged values same as ρ, the velocity component u_i in x_i direction is defined as the mass-averaged value. The acceleration components due to external force and surface tension are given by f_i and $f_{s,i}$ respectively, while $f_{s,i}$ is neglected in the present computations.

Discretization and computational method

Numerical algorithms are almost similar to the ones that have been proposed for incompressible fluids using collocated grid system (4). The computational procedures consist of three stages; prediction, pressure-calculation and correction stages.

In the prediction stage, the estimated velocity components are obtained at the cell center points. At this stage, the momentum equations, in which pressure variables are evaluated at the present computational step n, the velocity variables are discretized implicitly, which corresponds to the C-ISMAC method proposed to free-surface flows (5). The C-ISMAC method allows us to use larger time increment Δt than explicit methods, while higher-order spatial scheme is easily implemented. The convection terms are written in the preservation forms

and they are evaluated higher-order TVD schemes or the fifth-order FVM-QSI scheme that is advantageous in the computational accuracy, preservation and numerical stabilities.

In the MICS, the computational volumes occupied by solid bodies are also treated as incompressible fluids with different physical properties. The volume fraction of solid bodies in a single three-dimensional cell is evaluated with a sub-cell method (3). Since the tangential forces acting on solid bodies are evaluated through the diffusion terms in momentum equations, no complicated treatments for the boundaries are necessary.

At the pressure-calculation stage, the estimated cell-centered velocity components are spatially interpolated on the cell boundaries and pressure field is corrected so that the divergence of velocity vectors in a cell D should be sufficiently small. In order to correct the pressure field in this way, the C-HSMAC method (6) is utilized. In this method, firstly, the gradients of pressure variables, which are located at cell center points, are evaluated for the velocity components interpolated on cell boundaries. Then the pressure is corrected through the iterative computations with the following three equations until the divergence $|D^k|$ at k step of the iteration in each cell becomes less than the threshold value D_0.

$$\frac{\partial}{\partial x_i}\left(\frac{1}{\rho}\frac{\partial \phi^k}{\partial x_i}\right) = \frac{1}{\Delta t}\frac{\partial \hat{u}_i^k}{\partial x_i} \equiv \frac{1}{\Delta t}D^k \tag{4}$$

$$p^{k+1} = p^k + \phi^k \tag{5}$$

$$\hat{u}_i^{k+1} = \hat{u}_i^k - \frac{1}{\rho}\frac{\partial \phi^k}{\partial x_i}\Delta t \tag{6}$$

where superscript k is the step number of the iterative computation in the C-HSMAC method, $\hat{u}_i$ is the velocity components on cell boundaries. The discretized relationships of Eq. (4) form the linear system of ϕ and the numerical solutions can be derived by the BiCGSTAB method (7). When the divergence, or the error of fluid continuity D^k, becomes less than the threshold D_0 in all cells, the iterative computation is completed and the cell-centered velocity components are corrected with the obtained pressure variables in the correction stage.

The present C-HSMAC method for pressure computation allows us to deal with the flow field where the density distributions significantly change. Actually, it is applicable to the stably stratified two-layer flows in a rectangular tank where the densities of the upper and lower layers, ρ_u and ρ_l, are largely different. Fig.1 shows the relationship between the angular frequency σ of the standing waves arising on the two-layer interface and the ratio of densities $r_\rho = \rho_u/\rho_l$ in the stably stratified two-layer fluids, in which the small amplitude sinusoidal profile is initially given to the interface of two layers. While the density ratio r_ρ ranges from 0.8×10^{-3} to 1.0, the predicted angular frequencies agree well with the theoretical values, which are evaluated from the following relationship, in the wide range of r_ρ:

$$\sigma = \left[\frac{\pi g}{b}\cdot\frac{\rho_l - \rho_u}{\rho_u \coth\dfrac{\pi h_u}{b} + \rho_l \coth\dfrac{\pi h_l}{b}}\right]^{1/2} \tag{7}$$

where h_u and h_l are depths of upper and lower layers respectively, b is the horizontal length of the rectangular tank and g is the acceleration of gravity.

The fluid force acting on a solid body F_s is evaluated through the computational results described above (8). The fluid force in a single cell F_c is calculated through the terms included on the right hand side of momentum equations, which are external force, pressure and diffusion terms. The volume fraction of a solid body is evaluated with a sub-cell method. In the sub-cell method, as illustrated in Fig.2, a computational cell is divided into multiple smaller sub-cells and the number of the sub-cells included in the solid body is counted. The volume fraction is estimated with the number of sub-cells.

The fluid force F_s is obtained as the summation among all cells that include the solid body, $\sum f_{cs}F_c$, where f_{cs} is the volume fraction of the solid bodies in a cell.

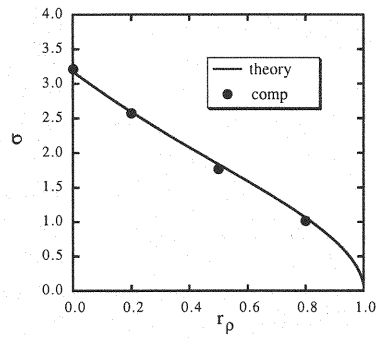

Fig. 1 Relationship between σ and r_ρ in standing waves of two-layer interface

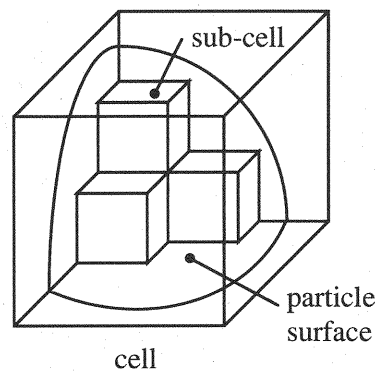

Fig. 2 Sub-cell method

The motions of solid bodies are predicted with the governing equations for translational and rotational motions. In these equations, the body-body and body-boundary contact forces are taken into account on the basis of a 3D DEM model (9), in addition to the fluid forces. With the position of solid bodies calculated at a new time step $n+1$, their new volume fraction in each cell is calculated and the physical properties are determined with the sub-cell method.

HYDRAULIC EXPERIMENTS AND ITS PREDICTIONS

Experimental flume and measuring method

The outline of the experimental flume is shown in Fig. 3. This flume has a wave generator, which is a flat plate that can be shifted continuously by the electric slider controlled by a computer. In the experiments, the value of the translational shift was 0.1 m and its moving speed was 0.4 m/s.

A rectangular step and four boxes are fixed in the flume. The height of the step h_s is 0.1 m, which is same as the depth of the initial static water h. The boxes B1 and B2, which correspond to the coastal levee and the land area, are set up on the step symmetrically in the flume. The waterway A between the boxes shows the river area, along with the wave flows run up in the experiment. The bottom height of the waterway A is equal to h_s and it is dry in the initial condition of the experiment. The geometries of the flume are $L0 = 0.64$ m, $L1 = 80$

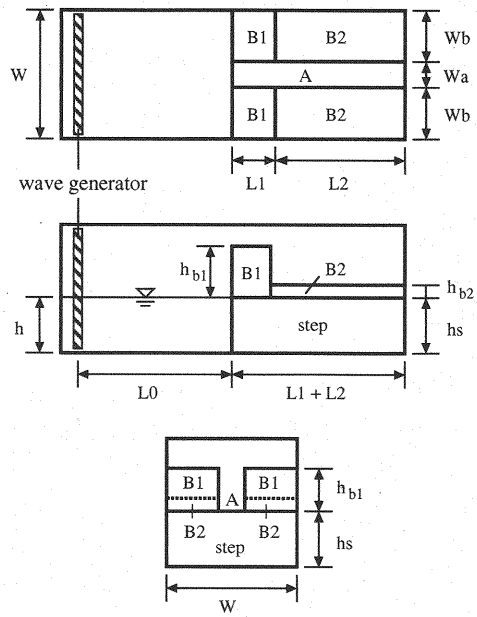

Fig. 3 Geometry of flume (plane, side and front views)

mm, $L2 = 0.56$ m, $W = 0.19$ m, $W_a = 30$ mm and $W_b = 80$ mm. The heights of the boxes are $h_{b1} = 0.1$ m and $h_{b2} = 10$ mm.

In the experiment, the generated waves collide with the boxes B1 and a part of the wave flow, entering between boxes B1, runs up along waterway A. No waves overflow boxes B1 in the present conditions. Some of the running-up flows into waterway A overflow on the boxes B2 and extend over the surfaces. In addition, the remaining running-up flows that reach the upstream end, which is a vertically fixed wall, are reflected on it and then toward in the downstream direction. In the experiments, the water was colored with dye and the running-up flows in waterway A and flooded flows on boxes B2 were visualized. The behaviors of the visualized flows were captured through the video camera set up above the flume.

Conditions of computations

The running-up wave flows and flooded flows were numerically simulated with 3D MICS. Since MICS enables us to deal with multiphase flows, water and air flows are simultaneously predicted, taking account that they are incompressible fluids with different physical properties.

The geometries of the computational volume are 1.28 m in length , 0.19 m in width and 0.20 m in height. The number of computational cells are $80 \times 24 \times 40$ in each direction. The convection terms included in the momentum equations and the mass-conservation equation are solved with a fifth-order TVD scheme (10). In the prediction stages of the numerical algorithms for momentum and mass-conservation equations, a C-ISMAC method (5) is used and it allows us to set $\Delta t = 5.0 \times 10^{-3}$ sec. The kinematic viscosities for water and air are 1.0×10^{-6} m^2/s and 1.0×10^{-5} m^2/s and their densities are 1.0×10^3 kg/m^3 and 1.0 kg/m^3 respectively. The linear system of the discretized pressure equations is solved with the BiCGSTAB method (7) and the threshold for the dot product of the residual vectors is set at 1.0×10^{-10}.

Comparison and applicability of the prediction method

The running-up wave flows along waterway A and flooded flows over boxes B2 are shown in Figs. 4 to 7, in which experimental and predicted results are compared. As shown in Fig.4, the first wave flow enters waterway A at about $t = 0.9$ sec. after the start of the wave generation. The wave flows immediately overflow on the top surfaces of boxes B2. The flooded flows on boxes B2 extend toward transverse and upstream directions. It is noted that the water depth of the front area is larger than the other region. In the computations, the fluid motions, including their turbulent components, are directly predicted. Thus, the non-symmetric flow behaviors are naturally reproduced in the predictions.

In addition to the flooded flows, the wave flow in waterway A still exists and runs up in the upstream direction. This wave flow increases its depth and overflows on both sides after it collides with the upstream wall, as shown in Figs.4 (f) to (h). Then the reflected wave flow proceeds in the downstream direction. It is possible that the similar flooded flows actually occur when the structures, such as closed flood gates, exist in a river. Moreover, in case that the reflected wave flow directing toward downstream direction arises, the reflected wave flow collides with the following running-up flows coming from a river mouth and the water depth becomes larger due to the interference of both waves.

The tendencies observed in the experimental results described above are reasonably reproduced in the predicted results as shown in Fig.5. The unsteady processes of the extension of the flooded flows and the reflection and interference of wave flows in the waterway are adequately simulated with the present method. In particular, the fact that the water depth of the front area in the flooded flows is larger than the other areas is also predicted in the computational results.

While general features of the experiments are suitably predicted, some discrepancies can be found between experiments and predictions regarding the distributions of very thin water layers on boxes B2. In the experiments, the thin water layers remain on the surfaces of boxes B2, while in the predictions they have disappeared. This effect is possibly related to the wettability of the box surfaces in experiments. The wettability is defined as the contact angle between a droplet of the liquid in thermal equilibrium on a horizontal surface. This effect is thought to be dominant in the smaller-scale experiments. Thus, it might be necessary to adopt the larger-scale experimental flume, in order to remove this effect.

The results after $t = 1.7$ s are shown in Figs.6 and 7. In the experiments, a large amount of water overflows on boxes B2 near the upstream end due to the collision of running-up wave flows with the wall. As shown in Fig.6 (c), the second wave flow enters the waterway A from the downstream side. This flow also floods over boxes B2 just after the entrance into waterway A, which is similar to the first wave flow.

Fig.7 shows the predicted results for the above experimental results. Compared with Figs.7 (a) to (d), it can be seen that the predicted velocity of the front area of the flooded regions is somewhat slower than the experiments. While the reason for this difference is not clear, it is possible that the vertical resolution of computational cell might not be sufficient. On the other hand, the entrance and overflow of the second wave flow are adequately predicted by the present method.

CONCLUSIONS

The three-dimensional computational method for multiphase flows, 3D MICS, has been developed and its applicabilities have been discussed for the running-up flows in a waterway caused by the generated waves. Hydraulic experiments have been conducted with a flume equipped with a wave generator and a step and boxes which simulate a waterway, coastal levees and the land areas. As a result of the computations with 3D MICS, it has been found that some features, such as the running-up flows in waterway A, the extension of the flooded flows on boxes B2, reflection on the upstream end wall and the entrance of the second wave flows, are successfully reproduced. While some discrepancies were found on the thin water layers and the speed of the extension of the flooded flows, it can be concluded that 3D MICS is generally applicable to the experimental results of the running-up flows and its flooded flows caused by tsunamis.

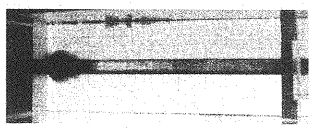

(a) $t = 0.9$ (s)

(b) $t = 1.0$ (s)

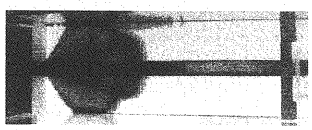

(c) $t = 1.1$ (s)

(d) $t = 1.2$ (s)

(e) $t = 1.3$ (s)

(f) $t = 1.4$ (s)

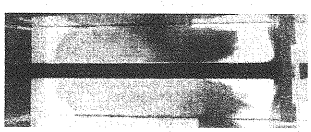

(g) $t = 1.5$ (s)

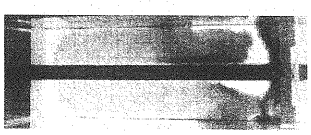

(h) $t = 1.6$ (s)

Fig. 4 Experimental results

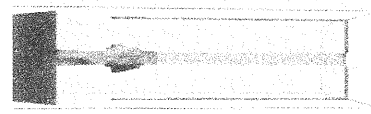

(a) $t = 0.9$ (s)

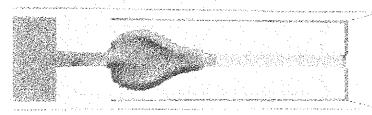

(b) $t = 1.0$ (s)

(c) $t = 1.1$ (s)

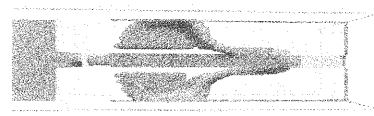

(d) $t = 1.2$ (s)

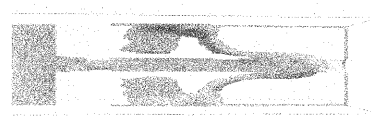

(e) $t = 1.3$ (s)

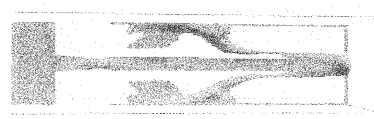

(f) $t = 1.4$ (s)

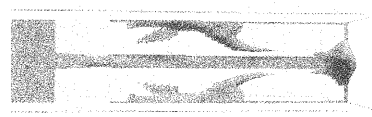

(g) $t = 1.5$ (s)

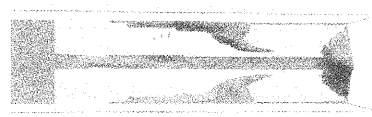

(h) $t = 1.6$ (s)

Fig. 5 Predicted results

(a) $t = 1.7$ (s)

(b) $t = 1.8$ (s)

(c) $t = 1.9$ (s)

(d) $t = 2.0$ (s)

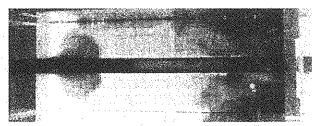

(e) $t = 2.1$ (s)

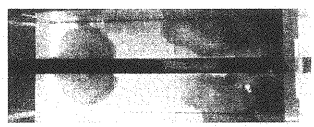

(f) $t = 2.2$ (s)

(g) $t = 2.3$ (s)

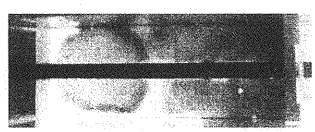

(h) $t = 2.4$ (s)

Fig. 6 Experimental results

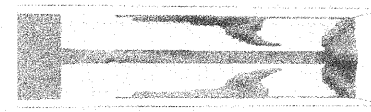

(a) $t = 1.7$ (s)

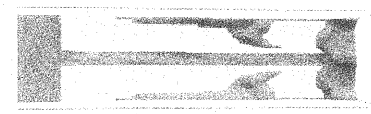

(b) $t = 1.8$ (s)

(c) $t = 1.9$ (s)

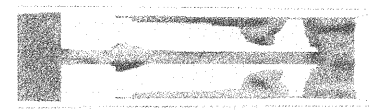

(d) $t = 2.0$ (s)

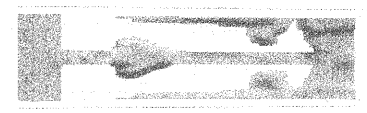

(e) $t = 2.1$ (s)

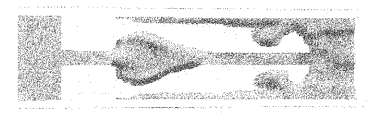

(f) $t = 2.2$ (s)

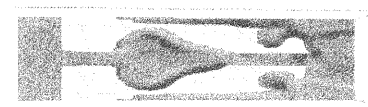

(g) $t = 2.3$ (s)

(h) $t = 2.4$ (s)

Fig. 7 Predicted results

REFERENCES

1. Liu, X., Sakai, S., Obara, T., Mikami, T., Iwama, S., Imamura, F. and Shuto, N.: Numerical simulation of tsunami run-up and tsunami-induced flood to a coastal urban area, *Proc. Coastal Eng., JSCE*, Vol. 48, No. (1), pp. 341–345, 2001.
2. Yasuda, H. and Watanabe, Y.: Numerical study on the propagation of tsunami in rivers, *Annual Journal of Hydraulic Engineering, JSCE*, Vol. 49, pp. 1327–1332, 2005.
3. Ushijima, S., Yamada, S., Fujioka, S. and Nezu, I.: Prediction method (3D MICS) for transportation of solid bodies in 3D free-surface flows, *Journals of JSCE*, Vol. 810/II-74, pp. 79–89, 2006.
4. Ushijima, S., Takemura, M. and Nezu, I.: Investigation on computational schemes for MAC methods with collocated grid system, *Journals of JSCE*, No. 719/II-61, pp. 11–19, 2002.
5. Ushijima, S. and Nezu, I.: Higher-order implicit method (C-ISMAC method) for incompressible flows with collocated grid system, *Journals of JSCE*, No. 719/II-61, pp. 21–30, 2002.
6. Ushijima, S., Okuyama, Y., Takemura, M. and Nezu, I.: Parallel computational method for pressure field in incompressible flows on 3D curvilinear coordinates, *Annual Journal of Hydraulic Engineering, JSCE*, Vol. 47, pp. 385–390, 2003.
7. Vorst, H. A. V. D.: BI-CGSTAB : A first and smoothly converging variant of BI-CG for the solution of nonsymmetric linear systems, *SIAM J. Sci. Stat. Comput.*, Vol. 13, pp. 631–644, 1992.
8. Ushijima, S., Takemura, M., Yamada, S. and Nezu, I.: Computational method for multiphase incompressible flows (MICS) and its applicability to particle-laden liquid flows, *Journals of JSCE*, No. 740/II-64, pp. 121–130, 2003.
9. Ushijima, S., Tanaka, N. and Yoneyama, N.: Lagrangian approach for solid-particles in gas-solid flows in a 3D complicated-shaped domain, *Annual Journal of Hydraulic Engineering, JSCE*, Vol. 43, pp. 515–520, 1999.
10. Yamamoto, S. and Daiguji, H.: Higher-order-accurate upwind schemes for solving the compressible Euler and Navier-Stokes equations, *Computers Fluids*, Vol. 22, No. 2/3, pp. 259–270, 1993.

APPENDIX-NOTATION

The following symbols are used in this paper:

D_0	= threshold for the error on fluid continuity;
D^k	= divergence of velocity at k step in a C-HSMAC method;
f_i	= acceleration of external force in x_i direction;
$f_{s,i}$	= acceleration of surface tension in x_i direction;
p	= volume-averaged pressure;
t	= time;
u_i	= mass-averaged velocity component in x_i direction;
$\hat{u}_i^k$	= cell-boundary velocity component at k step in C-HSMAC method;
x_i	= orthogonal coordinates;
Δt	= time increment;
μ	= volume-averaged coefficient of viscosity;
ρ	= volume-averaged fluid density;
ϕ^k	$= p^{k+1} - p^k$.

(Received July 31, 2006 ; revised September 19, 2006)